Journal of Power Sources 240 (2013) 636–643

Contents lists available at SciVerse ScienceDirect

Journal of Power Sources

journal homepage: www.elsevier.com/locate/jpowsour

Preparation of lithium ion conducting solid electrolyte of NASICON-type $Li_{1+x}Al_xTi_{2-x}(PO_4)_3$ ($x = 0.3$) obtained by using the mechanochemical method and its application as surface modification materials of $LiCoO_2$ cathode for lithium cell

Hideyuki Morimoto [a,*], Hiroyuki Awano [b], Junpei Terashima [b], Yohei Shindo [b], Shinji Nakanishi [b], Nobukiyo Ito [a], Kiyotaka Ishikawa [a], Shin-ichi Tobishima [a]

[a] Department of Chemistry and Chemical Biology, Graduate School of Engineering, Gunma University, 1-5-1 Tenjin-cho, Kiryu, Gunma 376-8515, Japan
[b] Toyota Motor Corporation, 1200, Mishuku, Susono, Shizuoka 410-1193, Japan

HIGHLIGHTS

- Lithium ion conductive LATP-modified $LiCoO_2$ cathodes were prepared.
- LATP-modified $LiCoO_2$ improved cycle performance.
- LATP-modified $LiCoO_2$ decreased charge transfer resistance.

ARTICLE INFO

Article history:
Received 11 March 2013
Received in revised form
24 April 2013
Accepted 10 May 2013
Available online 18 May 2013

Keywords:
Lithium-ion battery
$LiCoO_2$ cathode
Solid electrolyte
Lithium ion conductor
Milling

ABSTRACT

Amorphous a-LATP ($x = 0.3$) fine powder with the composition of $Li_{1+x}Al_xTi_{2-x}(PO_4)_3$ in $Li_2O-Al_2O_3-TiO_2-P_2O_5$ system was prepared directly from a mixture of Li_2O, γ-Al_2O_3, TiO_2, and P_2O_5 as starting materials, by using a mechanical milling (MM) technique at room temperature. A NASICON-type $Li_{1+x}Al_xTi_{2-x}(PO_4)_3$ ($x = 0.3$) (c-LATP ($x = 0.3$)) solid solution was obtained by the heat treatment of mechanochemically prepared amorphous a-LATP ($x = 0.3$) material. The sintered c-LATP ($x = 0.3$) pellet showed high lithium ion conductivity of the order of 10^{-4} S cm^{-1} at room temperature and activation energy of about 35 kJ mol^{-1}. The high-conducting lithium ion c-LATP ($x = 0.3$) solid electrolyte fine powders were investigated as surface modification materials of $LiCoO_2$ cathode in lithium cells using nonaqueous electrolyte solutions. The c-LATP ($x = 0.3$)-modified $LiCoO_2$ electrodes exhibited high capacity (*ca.* 180 mAh g^{-1}) and good cycle performance with a high charge cut-off potential of 4.5 V (vs. Li/Li$^+$) in lithium cell. The increase in the electrode/electrolyte interfacial resistance for the $LiCoO_2$ electrode modified with c-LATP ($x = 0.3$) fine powder was inhibited.

1. Introduction

$LiCoO_2$ positive electrodes have been used in most commercial lithium ion secondary batteries with nonaqueous electrolyte solutions. In the development of high-performance storage batteries, it is necessary to enhance the energy density of the lithium ion secondary battery. $LiCoO_2$ electrodes show good cycle performance with respect to Li metal at the charging voltage lower than 4.2 V. Although $LiCoO_2$ cathodes charged at voltages higher than 4.2 V (vs. Li/Li$^+$) show high capacities and make high voltage operation possible, their capacities decrease drastically during cycling [1,2]. Chen and Dahn reported that the improved cycling behavior was caused by the reduction in the contact area between $LiCoO_2$ and electrolyte [2]. The decrease in capacity was ascribed to the side reactions between nonaqueous electrolyte solutions and $LiCoO_2$ surface [2,3]. In fact, the oxidative decomposition of nonaqueous electrolyte solutions is enhanced significantly at voltages higher than 4.2 V (vs. Li/Li$^+$). As a result, the electrode/electrolyte interfacial resistance will increase, and the high-power performance of the cell will decrease remarkably.

Many researchers have reported that modifying $LiCoO_2$ with metal oxides, such as ZrO_2 [2,4–6], Al_2O_3 [4–7], SiO_2 [4,5], TiO_2 [6], and MgO [8–10], improves the electrode performance. For

* Corresponding author. Tel.: +81 277 30 1383; fax: +81 277 30 1380.
E-mail address: hmorimoto@gunma-u.ac.jp (H. Morimoto).

0378-7753/$ – see front matter © 2013 Elsevier B.V. All rights reserved.
http://dx.doi.org/10.1016/j.jpowsour.2013.05.039

example, $LiCoO_2$ modified with ZrO_2 has been reported to show better cycle performance than $LiCoO_2$, when charged at high voltage of 4.5 V (vs. Li/Li^+) [2]. With the modification with insulating oxide materials, enhancement in the life cycle is expected. However, they may hinder lithium ion transfer and cause increase in the interfacial resistance of electrodes and electrolytes. The modification agent, which has high lithium ion conductivity and inhibits the side reaction at the interface of electrolytes and electrodes, will enhance both the cycle stability and high-power performance.

Lithium-ion-conducting solid electrolytes with inorganic solids with high lithium ion conductivity at room temperature have been reported, such as NASICON-type $LiM_2(PO_4)_3$ (M = tetravalent cation, *e.g.*, Ti, Ge)-based ceramics composed of both MO_6 octahedra and PO_4 tetrahedra, which are linked by their corners to form a three-dimensional network structure [11–13]. $LiTi_2(PO_4)_3$-based solid electrolytes were prepared by a solid-state reaction in air. Their applications are electrochemical energy devices, such as all solid-state lithium secondary batteries [14,15] and lithium/air secondary batteries [16,17], because they exhibit lithium ion conductivity as high as 10^{-4} S cm^{-1} at room temperature [11–13] and are stable in air and water [16,17]. The conductivity of *ca.* $x = 0.3$ composition in the $Li_{1+x}Al_xTi_{2-x}(PO_4)_3$ (LATP) formula was the highest for the $LiTi_2(PO_4)_3$ system [13]. In addition, NASICON-type solid electrolytes are expected to show high electrochemical oxidative decomposition in lithium cells. For example, NASICON-type $LiGe_2(PO_4)_3$-based solid electrolytes have been reported to show high electrochemical oxidative potential of about 6 V (vs. Li/Li^+) [18]. Therefore, NASICON-type solid electrolytes are expected to show high electrochemical oxidative decomposition in lithium cells.

On the other hand, much attention has been paid to the mechanical milling (MM) technique using a high-energy ball mill as one of the new preparation procedures for inorganic solid electrolytes, such as ZrO_2-based [19] or Bi_2O_3-based oxide ion conductors [20], and Li_2S-based conductors with high lithium-ion conductivity [21–23]. The samples prepared mechanochemically by using MM processes are directly used as battery materials without pulverizing procedures, because they are obtained as fine powder. Hence, an increase in the contact interface of electrode and electrolyte is expected.

Here, we try to prepare a high-performance $LiCoO_2$ cathode modified with c-LATP ($x = 0.3$) solid-electrolyte fine powder that has a high lithium-ion conductivity, prepared by MM. In this study, amorphous (a-LATP ($x = 0.3$)) fine powder with the composition of

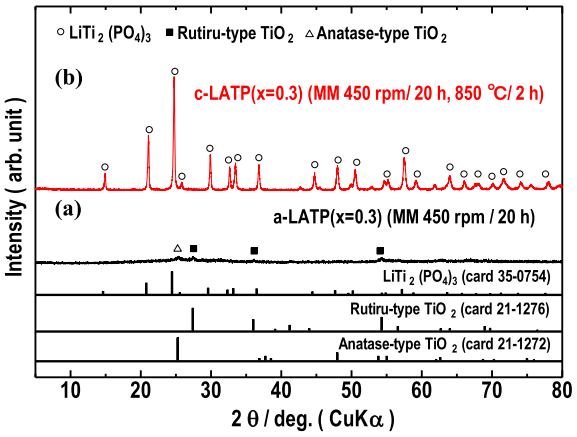

Fig. 1. XRD patterns of (a) a-LATP ($x = 0.3$) powder obtained by MM treatment for the mixture as starting materials and (b) c-LATP ($x = 0.3$) powder obtained by heat treatment of a-LATP ($x = 0.3$) powder after MM treatment.

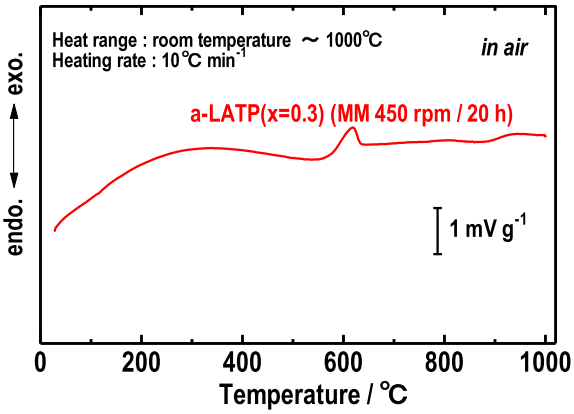

Fig. 2. DTA curve of a-LATP ($x = 0.3$) powder prepared by MM treatment for the mixture as starting materials.

$Li_{1+x}Al_xTi_{2-x}(PO_4)_3$ ($x = 0.3$) in Li_2O–Al_2O_3–TiO_2–P_2O_5 system was synthesized directly from a mixture of starting materials Li_2O, γ-Al_2O_3, TiO_2, and P_2O_5, using MM technique at room temperature. NASICON-type $Li_{1+x}Al_xTi_{2-x}(PO_4)_3$ ($x = 0.3$) (c-LATP ($x = 0.3$)) solid electrolyte with high lithium-ion conductivity was prepared by the heat treatment of a-LATP materials. Charge–discharge cycling behavior and electrode/electrolyte interphase impedance of c-LATP ($x = 0.3$)-modified $LiCoO_2$ electrodes were investigated for a charge cut-off potential of 4.5 V (vs. Li/Li^+) in a lithium cell using nonaqueous electrolyte solutions.

2. Experimental

2.1. Preparation of a-LATP and c-LATP powder

Reagent-grade γ-Al_2O_3, Li_2O, P_2O_5, and anatase-type TiO_2 were used as starting materials. Mechanical milling treatment was

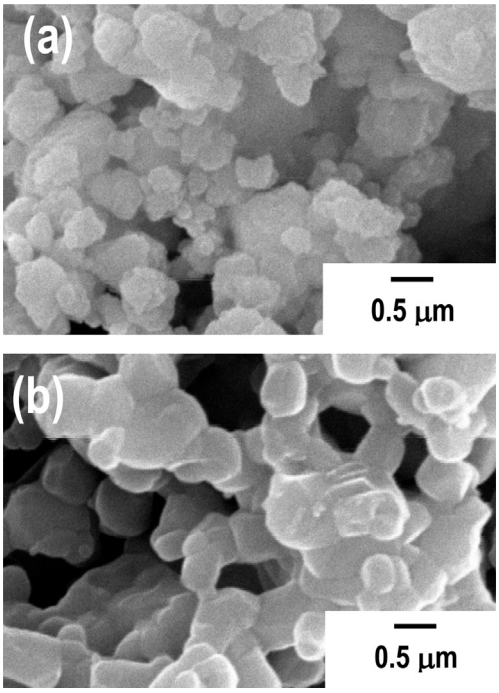

Fig. 3. SEM images of (a) a-LATP ($x = 0.3$) powder prepared by MM and (b) c-LATP ($x = 0.3$) powder obtained by heat treatment of a-LATP ($x = 0.3$) powder at 850 °C for 2 h.

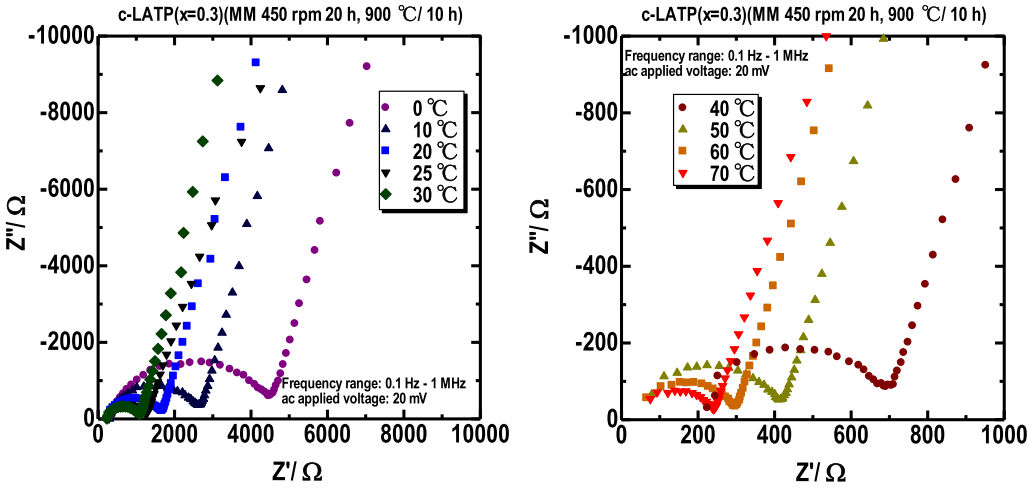

Fig. 4. Nyquist plots of sintered c-LATP ($x = 0.3$) pellet obtained from pelletized a-LATP ($x = 0.3$) by sintering at 900 °C for 10 h.

carried out on the mixture of starting materials using a planetary ball mill (Fritsch, p-7) with a rotation speed of 450 rpm at room temperature in dry Ar atmosphere. Stainless steel pots and zirconia balls were used for planetary ball milling. The volumes of pots and the number of balls were 45 mL and 10, respectively. Balls-to-mixture weight ratios ranging from 10:1 to 20:1 were employed using balls with diameters of 10 mm. X-ray diffraction (XRD) measurements (Rigaku, MiniFlex) with Cu Kα radiation were performed to identify the crystalline phase of the product powder obtained by mechanical milling treatment. The measurement conditions were set as follows: tube voltage was 30 kV; tube current, 15 mA; scan speed, 2° min^{-1}; diffraction angle, 5°–80°; and sampling width, 0.01°. Differential thermal analysis (DTA) (Rigaku, Thermo plus TG8120) measurement was performed to the powder obtained by MM treatment under air flow from room temperature to 1000 °C at a 10 °C min^{-1} heating rate. Particle size and morphology was estimated by SEM (JEOL, JSM-6510) observations.

2.2. Preparation of sintered c-LATP ($x = 0.3$) pellet and its conductivity measurements

A pellet-type sample was obtained by cold-pressing the amorphous powder (a-LATP ($x = 0.3$)) prepared by mechanical milling. The sample was sintered at 900 °C for 10 h in air. Electrical conductivity was measured for sintered c-LATP ($x = 0.3$) pellets with the diameter and thickness of 10 mm and about 1 mm, respectively. Au paste was applied over the pellets, and the pellets were then calcined at 850 °C for 2 h to prepare the electrodes. Then, AC impedance measurement was carried out in air using an impedance analyzer (Ivium, IviumStat) in the temperature range of 25–70 °C. The frequency range and applied voltage were 0.1 Hz–1 MHz and 20 mV, respectively.

2.3. Cell preparation and electrochemical measurements

Charge/discharge measurements for the cycle performance at constant current densities of 0.2 mA cm^{-2} during the first cycle and 0.5 mA cm^{-2} from the second cycle to the last cycle were carried out for the 2032 coin cells at room temperature by using a battery test system (Hokuto Denko, HJ1001SM8). These cells have a lithium metal counter electrode (Honjo chemical, lithium foil of 0.5 mm thickness) and a working electrode. The working electrodes were fabricated from $LiCoO_2$ or mechanically milled c-LATP ($x = 0.3$) powder mixed with $LiCoO_2$ (85 wt%), acetylene black (AB, 5 wt%), and polyvinylidene fluoride (PVDF, 10 wt%). In this experiment, the mechanically milled NASICON powder and $LiCoO_2$ were manually mixed by pestle and agate mortar at room temperature. The contents of c-LATP ($x = 0.3$) vs. $LiCoO_2$ were 1, 5, and 20 wt%. Next, these mixtures and acetylene black were again mixed manually. The powder was mixed with PVDF binder solution with 1-methyl-2-pyrrolidone (NMP) as solvent. This slurry was painted on the Al sheet of current collector and dried at 80 °C. It was pressed and dried in vacuum at 120 °C. The electrolyte was 1 mol dm^{-3} $LiPF_6$ in solvent mixture of ethylene carbonate (EC) and ethyl methyl carbonate (EMC) (3:7 volume ratio). Charge–discharge measurements were carried out at the cut-off potential range from 3.0 to 4.5 V versus Li/Li^+ at room temperature. AC impedance spectroscopy measurements for the cells were carried out by using an impedance analyzer (Ivium, IviumStat). The frequency range and applied voltage were 10 mHz–100 kHz and 5 or 20 mV, respectively.

3. Results and discussion

Fig. 1(a) shows the XRD pattern of a-LATP ($x = 0.3$) powder obtained by MM treatment of the mixture of starting materials. The peaks of the starting materials mostly disappeared and halo pattern

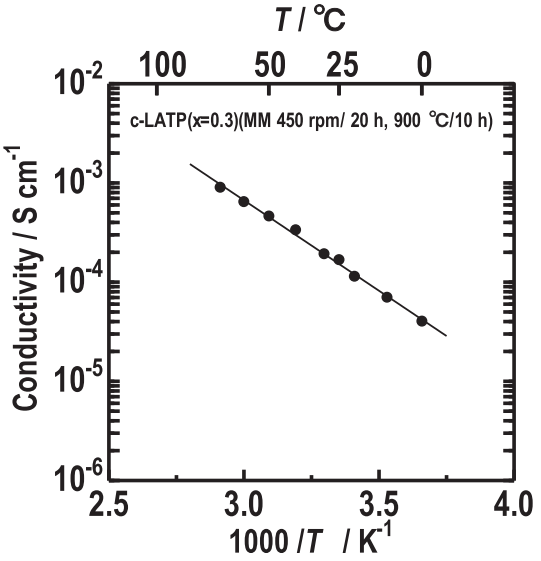

Fig. 5. Arrhenius plots of the electrical conductivities of sintered c-LATP ($x = 0.3$) pellet.

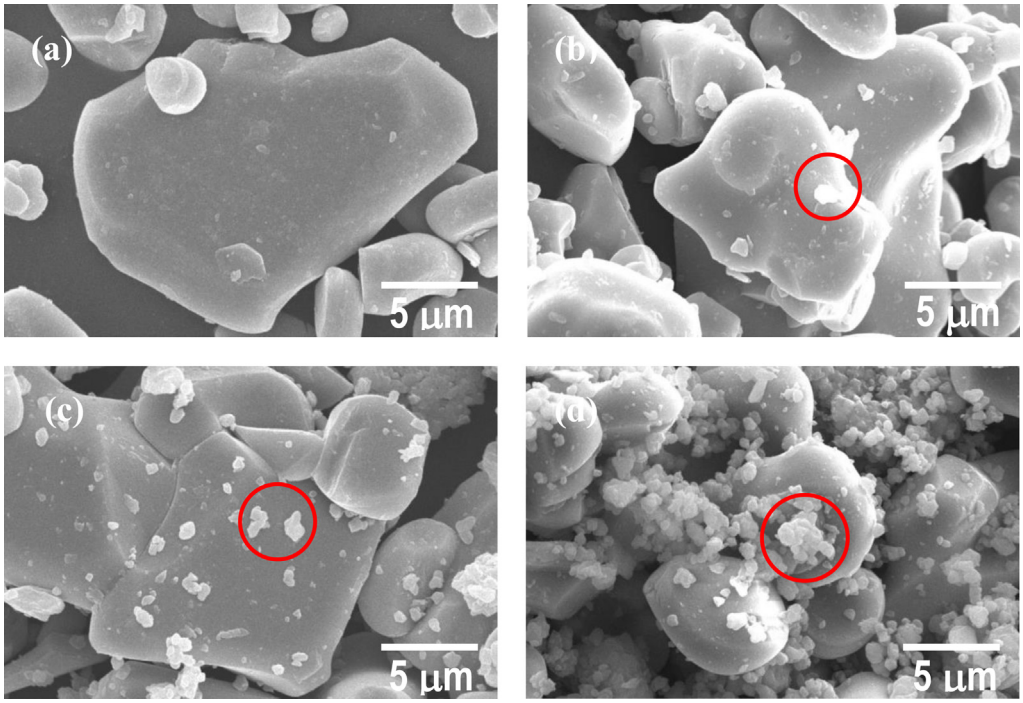

Fig. 6. SEM images of the mixture of $LiCoO_2$ and c-LATP ($x = 0.3$) powder in agate mortar [(a) $LiCoO_2$, (b) 1 wt% c-LATP ($x = 0.3$), (c) 5 wt% c-LATP ($x = 0.3$), (d) 20 wt% c-LATP ($x = 0.3$)].

is basically observed after milling for 20 h although the peaks due to anatase-type TiO_2 and rutile-type TiO_2 are very slightly observed. The amorphous phase will be formed by the mechanochemical reaction by using γ-Al_2O_3, Li_2O, P_2O_5, and anatase-type TiO_2 as a starting material. Amorphous material (a-LATP ($x = 0.3$)) in the Li_2O–Al_2O_3–TiO_2–P_2O_5 system will be synthesized at room temperature using the MM method. Fig. 1(b) shows the XRD pattern of c-LATP ($x = 0.3$) powder after the heat treatment of a-LATP ($x = 0.3$) powder at 850 °C for 2 h, showing the diffraction pattern assigned to $LiTi_2(PO_4)_3$ compound with NASICON-type structure. Fig. 2 shows the DTA curve of a-LATP ($x = 0.3$) powder. An exothermic peak is observed near 600 °C (exothermic onset temperature: 575 °C) during the heating processes. This result is assigned to the crystallization of amorphous material, and it indicates the validity

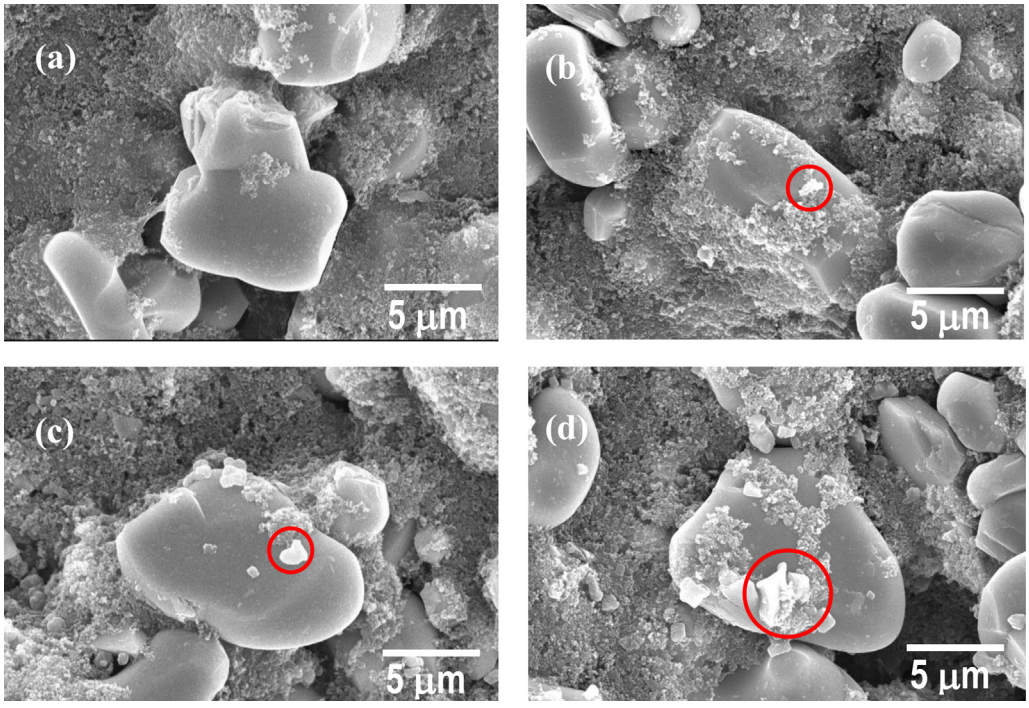

Fig. 7. SEM images of c-LATP ($x = 0.3$)-modified $LiCoO_2$ electrodes [(a) $LiCoO_2$, (b) 1 wt% c-LATP ($x = 0.3$), (c) 5 wt% c-LATP ($x = 0.3$), and (d) 20 wt% c-LATP ($x = 0.3$)].

to the results of XRD measurements shown in Fig. 1(a) and (b). Fig. 3 shows the SEM images of (a) a-LATP ($x = 0.3$) powder prepared by MM and (b) c-LATP ($x = 0.3$) powder obtained by heat treatment of a-LATP ($x = 0.3$) powder at 850 °C for 2 h. The roundish particles with diameter less than 1 μm are observed for a-LATP ($x = 0.3$) powder in Fig. 3(a). Probably existence of amorphous particles is suggested. It will be because it has an isotropic configuration. On the other hand, from the SEM image of c-LATP ($x = 0.3$) powder in Fig. 3(b), some square particles are observed by the heat treatment of a-LATP ($x = 0.3$) powder. Such results also suggest the crystallization of amorphous material.

Fig. 4 shows the results of the AC impedance measurements of sintered c-LATP ($x = 0.3$) pellet obtained from pelletized a-LATP ($x = 0.3$) by sintering at 900 °C for 10 h. The diameters of the semicircles of Nyquist plots decreased with the increase in the measurement temperature. The diameters are considered to be the resistance (R) of the sample, and the electrical conductivities are calculated from the following formula.

$$\sigma = (1/R)(L/S), \quad (1)$$

where L and S are the thickness and cross-sectional area of sintered pellet sample, respectively.

Fig. 5 shows Arrhenius plots of the electrical conductivities of sintered c-LATP ($x = 0.3$) pellet. The sintered c-LATP ($x = 0.3$) pellet shows high conductivity of the order of 10^{-4} S cm^{-1} at room temperature. The total conductivity of bulk and grain boundary is *ca.* 1.5×10^{-4} S cm^{-1} at 25 °C. The conductivities for the sintered sample follow the Arrhenius-type equation:

$$\sigma = \sigma_0(-E_a/RT), \quad (2)$$

where E_a is the activation energy for conduction, σ_0 is the pre-exponential factor, and R is the gas constant. The activation energy of the c-LATP ($x = 0.3$) sample is calculated to be about 35 kJ mol^{-1}, which is in good agreement with that of $Li_{1+x}Al_xTi_{2-x}(PO_4)_3$ ($x = 0.3$) ceramics obtained by solid reaction method [13].

Fig. 6 shows the SEM images of the powder obtained by mixing of $LiCoO_2$ and c-LATP ($x = 0.3$) powder in agate mortar [(a) $LiCoO_2$, (b) 1 wt% c-LATP ($x = 0.3$), (c) 5 wt% c-LATP ($x = 0.3$), (d) 20 wt% c-LATP ($x = 0.3$)]. The images demonstrate that c-LATP ($x = 0.3$) particles are scattered on the surface of $LiCoO_2$ particles. It is observed that the surface of $LiCoO_2$ particles was further coated with the increase in c-LATP ($x = 0.3$) powder. Fig. 7 shows the SEM images of c-LATP ($x = 0.3$)-modified $LiCoO_2$ electrodes [(a) $LiCoO_2$, (b) 1 wt% c-LATP ($x = 0.3$), (c) 5 wt% c-LATP ($x = 0.3$), and (d) 20 wt% c-LATP ($x = 0.3$)], which indicate that both c-LATP ($x = 0.3$) and AB powder with PVDF binder modified the surface of $LiCoO_2$ particles. These solid materials function as electric conduction path for electrons and ions, and they will surely prevent the direct contact of $LiCoO_2$ particles with the liquid electrolyte in the cell.

Fig. 8 shows the 1st and 30th charge/discharge curves of c-LATP ($x = 0.3$)-modified $LiCoO_2$ electrodes. The horizontal axis (mAh g^{-1}) is based on the weight of $LiCoO_2$. $LiCoO_2$ electrodes with and without c-LATP ($x = 0.3$) exhibited similar polarization behaviors at the 1st cycle. The discharge curves above the charge cut-off potential of 4.5 V exhibit the high capacity of *ca.* 180 mAh g^{-1}. At the 30th cycle, $LiCoO_2$ electrode yields larger polarization than $LiCoO_2$ electrodes with c-LATP ($x = 0.3$). Fig. 9 shows the cycle performance of c-LATP ($x = 0.3$)-modified $LiCoO_2$ electrodes. $LiCoO_2$ electrodes with c-LATP ($x = 0.3$) reduce the capacity degradation of $LiCoO_2$. $LiCoO_2$ electrodes with 5 and 20 wt% c-LATP ($x = 0.3$) exhibit high capacities and good cycle performance during 50 cycles. Lithium-ion-conducting c-LATP ($x = 0.3$) particles may inhibit the oxidative decomposition of electrolytes at the $LiCoO_2$ particle surface without preventing the lithium ion transfer.

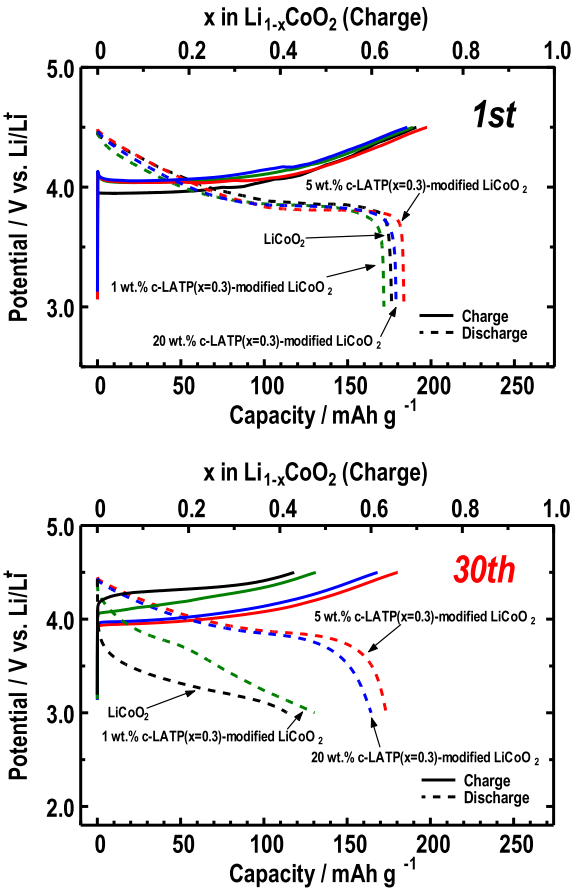

Fig. 8. 1st and 30th charge/discharge curves of c-LATP ($x = 0.3$)-modified $LiCoO_2$ electrodes.

The electrode/electrolyte interfacial resistance was investigated using the AC impedance technique. Fig. 10 shows the Nyquist plots of Li/c-LATP ($x = 0.3$)-modified $LiCoO_2$ cells at 25 °C after the 2nd and 5th charge. After two charge cycles, two semicircles were observed in Nyquist plots for all electrodes. In this paper, the semicircles for high- and middle-frequency ranges of AC impedance measurements for Li/$LiCoO_2$ cells were attributed on the basis of Refs. [24–27] to solid electrolyte interphase (SEI) or surface film

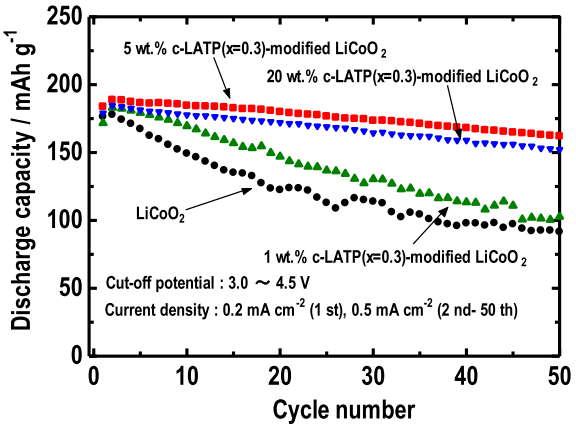

Fig. 9. Cycle performance of c-LATP ($x = 0.3$)-modified $LiCoO_2$ electrodes.

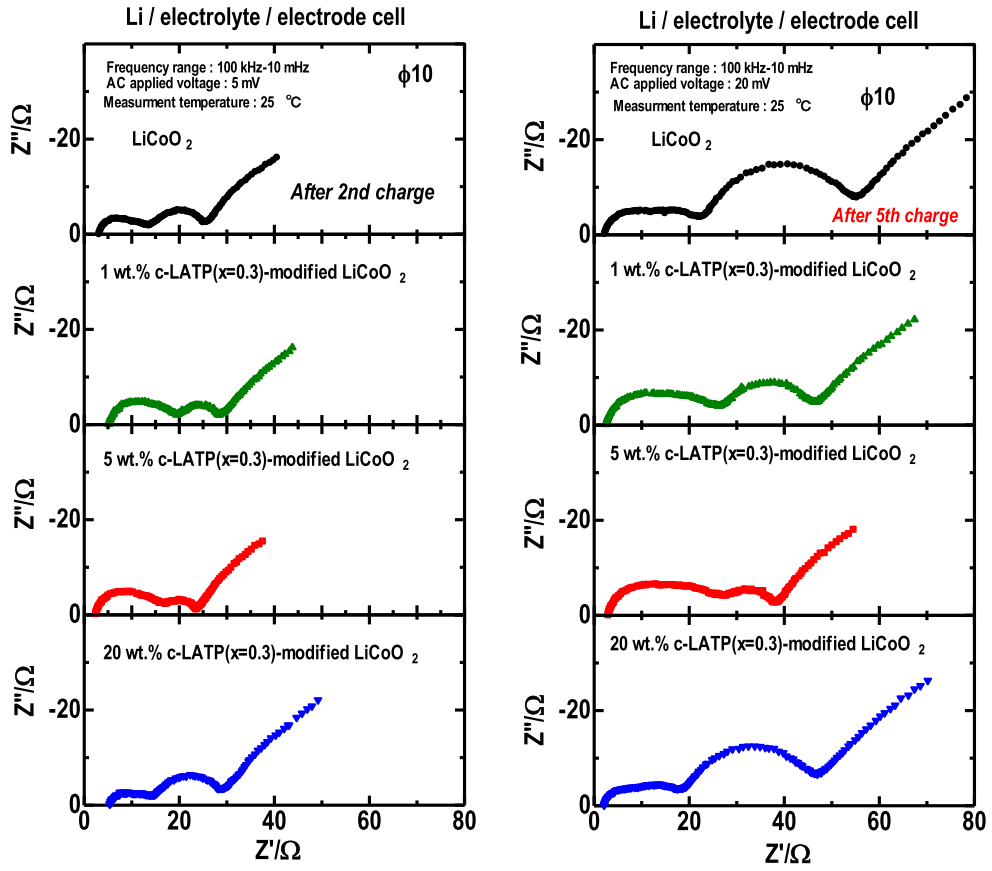

Fig. 10. Nyquist plots of Li/c-LATP ($x = 0.3$)-modified $LiCoO_2$ cells at 25 °C after the 2nd and 5th charge.

resistance and charge transfer resistance (R_{ct}), respectively. For high-frequency range, the 1 and 5 wt% c-LATP ($x = 0.3$)-modified $LiCoO_2$ electrodes show slightly larger semicircles compared to $LiCoO_2$ electrode. On the other hand, 20 wt% c-LATP ($x = 0.3$)-modified electrode shows smaller semicircle compared to $LiCoO_2$ electrode. For middle-frequency range, the diameter of the semicircle for 5 wt% c-LATP ($x = 0.3$)-modified $LiCoO_2$ electrode is the smallest among all electrodes. After the 5th charge cycle, the

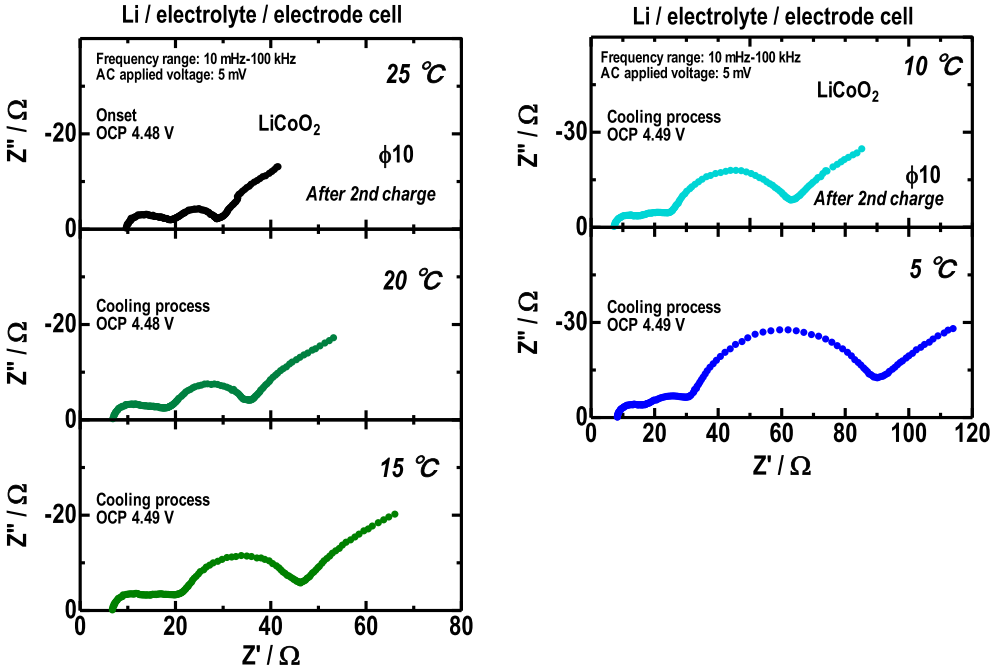

Fig. 11. Temperature dependence (5–25 °C) of the Nyquist plots of Li/$LiCoO_2$ cell after 2nd charge.

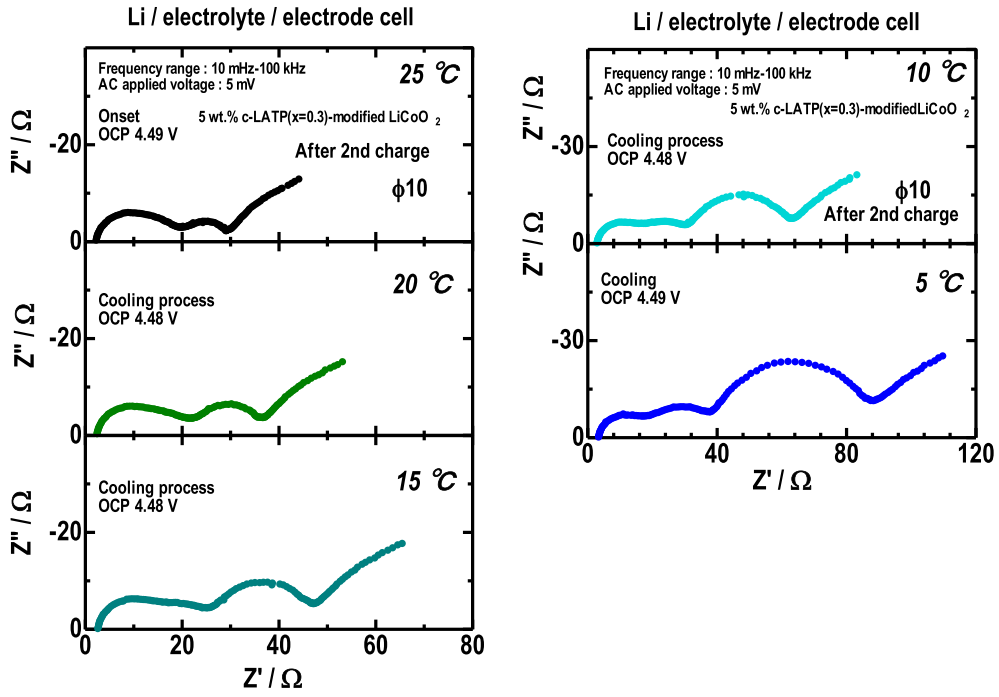

Fig. 12. Temperature dependence (5–25 °C) of the Nyquist plots of Li/5 wt% c-LATP ($x = 0.3$)-modified $LiCoO_2$ cell 2nd charge.

diameters of the semicircles of both high- and middle-frequency ranges are larger than after the 2nd charge cycle. The semicircle of the middle-frequency range for 5 wt% c-LATP ($x = 0.3$)-modified $LiCoO_2$ electrodes remains almost unchanged after the 2nd charge cycle. It is suggested that c-LATP ($x = 0.3$)-modified $LiCoO_2$ electrode inhibits the increase in charge transfer resistance. As a result, c-LATP ($x = 0.3$)-modified $LiCoO_2$ electrodes can inhibit the capacity decrease during the charge/discharge cycle. The decay of the positive electrode active material upon side reactions, such as the attack of HF on the active material, may be prevented at the interphase of electrolyte and electrode. In addition, it is found that the effects of modification of c-LATP ($x = 0.3$) can be evaluated using the AC impedance technique for charged cells during the early cycles.

We examined the temperature dependence of AC impedance measurements of the cell after the charge. Figs. 11 and 12 show the temperature dependence (5–25 °C) of the Nyquist plots of Li/$LiCoO_2$ and Li/5 wt% c-LATP ($x = 0.3$)-modified $LiCoO_2$ cells after the 2nd charge. Open circuit potentials (OCP) of the cells before the AC impedance measurements were stable at 4.48 or 4.49 V (vs. Li/Li^+). The charge transfer resistances increase clearly with decreasing measurement temperature. Fig. 13 shows the Arrhenius plots for the charge transfer resistances obtained from the Nyquist plots in Figs. 11 and 12. The activation energies for the charge transfer resistance of $LiCoO_2$ and c-LATP ($x = 0.3$)-modified $LiCoO_2$ electrodes are 61 and 55 kJ mol^{-1}, respectively. It is suggested that the c-LATP ($x = 0.3$)-modification of $LiCoO_2$ electrode decreases the activation energy for the charge transfer resistance. A new phase may be formed on the electrode/electrolyte interphase.

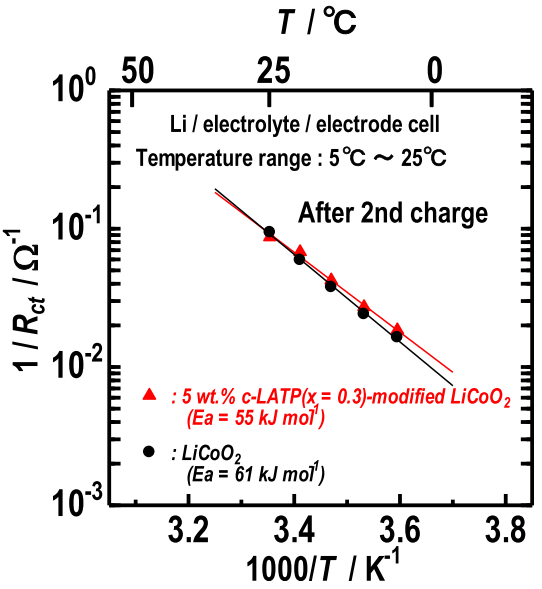

Fig. 13. Arrhenius plots for the charge-transfer resistances of Li/$LiCoO_2$ cell and Li/5 wt % c-LATP ($x = 0.3$)-modified $LiCoO_2$ cell after 2nd charge.

4. Conclusions

Amorphous (a-LATP ($x = 0.3$)) fine powder with the composition of $Li_{1+x}Al_xTi_{2-x}(PO_4)_3$ ($x = 0.3$) in the Li_2O–Al_2O_3–TiO_2–P_2O_5 system was prepared directly from a mixture of starting materials using a mechanical milling (MM) technique at room temperature. NASICON-type $Li_{1+x}Al_xTi_{2-x}(PO_4)_3$ ($x = 0.3$) (c-LATP ($x = 0.3$)) solid solution was formed close to 600 °C by the heat treatment of a-LATP ($x = 0.3$). The sintered c-LATP ($x = 0.3$) pellet, obtained by sintering of a-LATP ($x = 0.3$) at 900 °C for 10 h showed high conductivity on the order of 10^{-4} S cm^{-1} at room temperature. The c-LATP ($x = 0.3$) fine powder-modified $LiCoO_2$ electrodes exhibited high capacity (around 180 mAh g^{-1}) and good cycle performance at a high charge cut-off potential of 4.5 V (vs. Li/Li^+) in lithium cell. It is suggested that the c-LATP ($x = 0.3$)-modified $LiCoO_2$ electrode inhibits the increase in charge transfer resistance and decreases the activation energy for the charge transfer resistance of $LiCoO_2$ electrode. The high lithium ion conductive c-LATP ($x = 0.3$) solid electrolytes are promising as modification agents for the modifying

the surface of particles of high-energy-density positive electrode materials that need high charge voltage.

References

[1] J. Cho, C. Kim, S.I. Yoo, Electrochem. Solid-State Lett. 3 (2000) 362.
[2] Zhaohui Chen, J.R. Dahn, Electrochem. Solid-State Lett. 5 (10) (2002) A213.
[3] G.G. Amatucci, J.M. Tarascon, L.C. Klein, Solid State Ionics 83 (1996) 167.
[4] Z. Chen, J.R. Dahn, Electrochem. Acta 49 (2004) 1079.
[5] Z. Chen, J.R. Dahn, Electrochem. Solid-State Lett. 6 (11) (2003) A221.
[6] A.M. Kannan, L. Rabenberg, A. Manthiram, Electrochem. Solid-State Lett. 6 (1) (2003) A16.
[7] S. Oh, J.K. Lee, D. Byun, W.I. Cho, B.W. Cho, J. Power Sources 132 (2004) 249.
[8] M. Mladenov, R. Stoyanova, E. Zhecheva, S. Vassilev, Electrochem. Commun. 3 (2001) 410.
[9] H. Zhao, L. Gao, W. Qiu, X. Zhang, J. Power Sources 132 (2004) 195.
[10] Y. Iriyama, H. Kurita, I. Yamada, T. Abe, Z. Ogumi, J. Power Sources 137 (2004) 111.
[11] H. Aono, E. Sugimoto, Y. Sadaoka, N. Imanaka, G. Adachi, J. Electrochem. Soc. 136 (1989) 590.
[12] H. Aono, E. Sugimoto, Y. Sadaoka, N. Imanaka, G. Adachi, J. Electrochem. Soc. 137 (1989) 1023.
[13] H. Aono, E. Sugimoto, Y. Sadaoka, N. Imanaka, G. Adachi, J. Electrochem. Soc. 140 (7) (1993) 1827.
[14] Y. Iriyama, C. Yada, T. Abe, Z. Ogumi, K. Kikuchi, Electrochem. Commun. 8 (2006) 1287.
[15] C. Yada, Y. Iriyama, T. Abe, K. Kikuchi, Z. Ogumi, Electrochem. Commun. 11 (2009) 413.
[16] N. Imanishi, S. Hasegawa, T. Zhang, A. Hirano, Y. Takeda, O. Yamamoto, J. Power Sources 185 (2008) 1392.
[17] S. Hasegawa, N. Imanishi, T. Zhang, J. Xie, A. Hirano, Y. Takeda, O. Yamamoto, J. Power Sources 189 (2009) 371.
[18] X. Xu, Z. Wen, X. Wu, X. Yang, Z. Gu, J. Am. Ceram. Soc. 90 (9) (2007) 2802.
[19] D. Michel, F. Faudot, E. Gaffet, L. Mazerolles, J. Am. Ceram. Soc. 76 (11) (1993) 2884.
[20] T. Esaka, S. Takai, N. Nishimura, Denki Kagaku (Electrochemistry) 64 (1996) 1012.
[21] H. Morimoto, H. Yamashita, M. Tatsumisago, T. Minami, J. Am. Ceram. Soc. 82 (1999) 1352.
[22] M. Tatsumisago, H. Morimoto, H. Yamashita, T. Minami, Solid State Ionics 136-137 (2000) 483.
[23] A. Hayashi, S. Hama, H. Morimoto, M. Tatsumisago, T. Minami, J. Am. Ceram. Soc. 84 (2001) 477.
[24] S.S. Zhang, K. Xu, T.R. Jow, Electrochem. Solid-State Lett. 5 (5) (2002) A29.
[25] S.S. Zhang, K. Xu, T.R. Jow, J. Electrochem. Soc. 149 (2002) A1521.
[26] K.M. Shaju, G.V. Subba Rao, B.V.R. Chowdari, J. Electrochem. Soc. 150 (2003) Al.
[27] Y.-K. Sun, J.-M. Han, S.-T. Myung, S.-W. Lee, K. Amine, Electrochem. Commun. 8 (2006) 821.